Check for updates

Fabrication of high performance TFN membrane containing NH₂-SWCNTs *via* interfacial regulation

Qing Kong,[a] Hang Xu, [ID][a] ChenWei Liu,*[b] Guang Yang,[c] Mingmei Ding, [ID] *[a] Wen Yang,[a] Tao Lin, [ID][a] Wei Chen,[a] Stephen Gray [ID][c] and Zongli Xie [ID][d]

A high-flux thin film nanocomposite (TFN) nanofiltration (NF) membrane for low pressure operation (3.5 bar) was fabricated by blending purified amino-functionalized single-walled carbon nanotubes (NH₂-SWCNTs) with piperazine (PIP) as aqueous phase monomers through interfacial polymerization (IP). The surface properties and structures of the polyamide (PA) active layer were suitably tailored by introducing different amounts of NH₂-SWCNTs into the PA layer. It was found that the homogeneous incorporation of NH₂-SWCNTs facilitated a more integral PA layer along with improved roughness, hydrophilicity, and surface charge of the modified membranes, which could be validated by membrane characterisation including SEM, AFM, ATR-FTIR, XPS, zeta potential and water contact angle measurements. Based on cross-flow NF tests, the optimized ultra-thin NH₂-SWCNT-TFN membranes with 0.002 wt% of NH₂-SWCNTs exhibited outstanding water permeability of up to 17.8 L m^{-2} h^{-1} bar^{-1}, 71.1% higher than that of the pristine membrane, along with high MgSO₄ rejection of 91.0% and Na₂SO₄ rejection of 96.34%. Meanwhile, NH₂-SWCNT-TFN membranes also showed excellent long-term stability and antifouling ability. This work demonstrates a facile strategy to fabricate a scalable, low-pressure and ultra-thin TFN membrane with excellent performance.

1. Introduction

In recent decades, the demand for freshwater has increased significantly owing to the growing world population, improved living standards, changing consumption patterns, and expanding irrigated agriculture.[1] Purifying diverse sources of water, such as brackish water, industrial effluents, and other contaminated water *via* membrane filtration, is a cost-effective way of increasing the supply of freshwater.[2] Recently, nanofiltration (NF) membranes have been accepted and popularised globally owing to their relatively high water flux, high rejection of divalent ions, easy operation, and long service life. Thin-film composite (TFC) membranes, as a state-of-the-art NF membrane, are fabricated by forming an ultra-thin separation polyamide (PA) layer on a porous support, such as polysulfone (PSF) or polyethersulfone, *via* an interfacial polymerization (IP) reaction.[3,4] The PA layer acting as a rejecting layer plays a vital role in selectively excluding salt ions from water, while the support film provides sufficient mechanical integrity.[5]

Despite their excellent separation performances, TFC NF membranes face two major challenges that limit their wider application: 'trade-off' phenomenon between membrane water flux and separation capability, as well as high operation pressure (between 6 and 30 bars) to achieve the desired pure water flux.[6] To solve these two problems, extensive research has been conducted on the development of advanced materials and technologies to improve the permeability of NF membranes while maintaining high multivalent salt retention capacity at low pressures. On the one hand, according to the classic Hagen–Poiseuille equation,[7] one viable strategy is to have a selective layer as thin as possible to reduce the resistance to water transport along with appropriate pore sizes to obtain excellent rejection. On the other hand, it is imperative to improve the hydrophilicity and roughness of the membrane surface to facilitate interaction between the membrane and water molecules, thereby enhancing permeance.[8,9] However, it remains challenging to synchronously regulate the hydrophilicity and roughness of the membrane, as well as to decrease the thickness of the PA active layer without introducing defects.

Among various methods, the induction of nanomaterials into the PA layer has been proven to be a promising strategy to design highly effective membranes.[10] A series of novel thin-film nanocomposite (TFN) NF membranes has been constructed *via* the incorporation of various types of nanomaterials including metal–organic framework nanoparticles such as ZIF-8,[11] carbon-based nanomaterials such as carbon nanotubes (CNTs)[12] and

[a]Key Laboratory of Integrated Regulation and Resource Development on Shallow Lake of Ministry of Education, College of Environment, Hohai University, Nanjing 210098, China. E-mail: mingmei.ding@hhu.edu.cn

[b]Nanjing Institute of Environmental Sciences of the Ministry of Ecology and Environment, Nanjing 210042, China. E-mail: lcw@nies.org

[c]Institute of Sustainable Industries and Liveable Cities, Victoria University, P. O. Box 14428, Melbourne, Victoria 8001, Australia

[d]CSIRO Manufacturing, Private Bag 10, Clayton South, Vic. 3169, Australia

graphene oxide,[13] metal nanoparticles comprising silver,[14] metal oxide nanoparticles comprising TiO_2,[15] covalent organic framework nanoparticles,[16] and nano-scaffolds such as tannic acid/Fe^{3+}.[17] Nanomaterials with large surface areas and significant quantities of functional groups exhibit superior anti-biofouling[18] and anti-bacterial[14] properties. As long as a small amount of the nanomaterial is used, the surface roughness and free volume of the selective layer increases. At the same time, the transport resistance decreases as hydrophilicity increases. As a result, the performance of the modified NF membrane is greatly improved.

Among all kinds of nanomaterials, CNT is one of the most fascinating and popular in research owing to its excellent properties such as smoothness and regularity,[19] ceramic-like stability, polymer-like flexibility,[20] mechanical strength, electrical/thermal conductivity,[21] biocidal capability,[22] and antioxidant ability.[23] However, the wide application of CNT is currently restricted by its low hydrophilicity,[24] poor dispersion properties and solubility in many common solvents,[25] along with weak interfacial interactions with the polymer matrix.[26] In

previous works, CNTs were incorporated into PA layers of NF membranes[27–35] through different ways, but the permeance was still unsatisfactory. Furthermore, there were limited reports in the preparation of low-pressure TFC NF membranes (below 4 bars, which could be easily operated with most pumps) using low contents of CNTs.

In this work, we report a facile and scalable method for the preparation of ultra-thin TFN NF membranes with thickness of about 30 nm by uniformly incorporating NH_2-SWCNTs into the PA active layer to obtain high permeation flux and excellent rejection rate under low pressure (3.5 bar). Different from the commonly used multi-walled carbon nanotubes, SWCNTs are composed of only one graphene cylinder which is beneficial to reducing the water transport resistance. Besides, the diameter of SWCNT is usually 0.7–2.0 nm which is favorable for the formation of ultra-thin PA layers.[36] Attaching polar functional group of NH_2 to the surface of SWCNT can effectively improve not only dispersion property but also hydrophilicity, stability, and chemical compatibility with other polymers, thereby overcoming the deficiencies of bare SWCNT. In the case of water
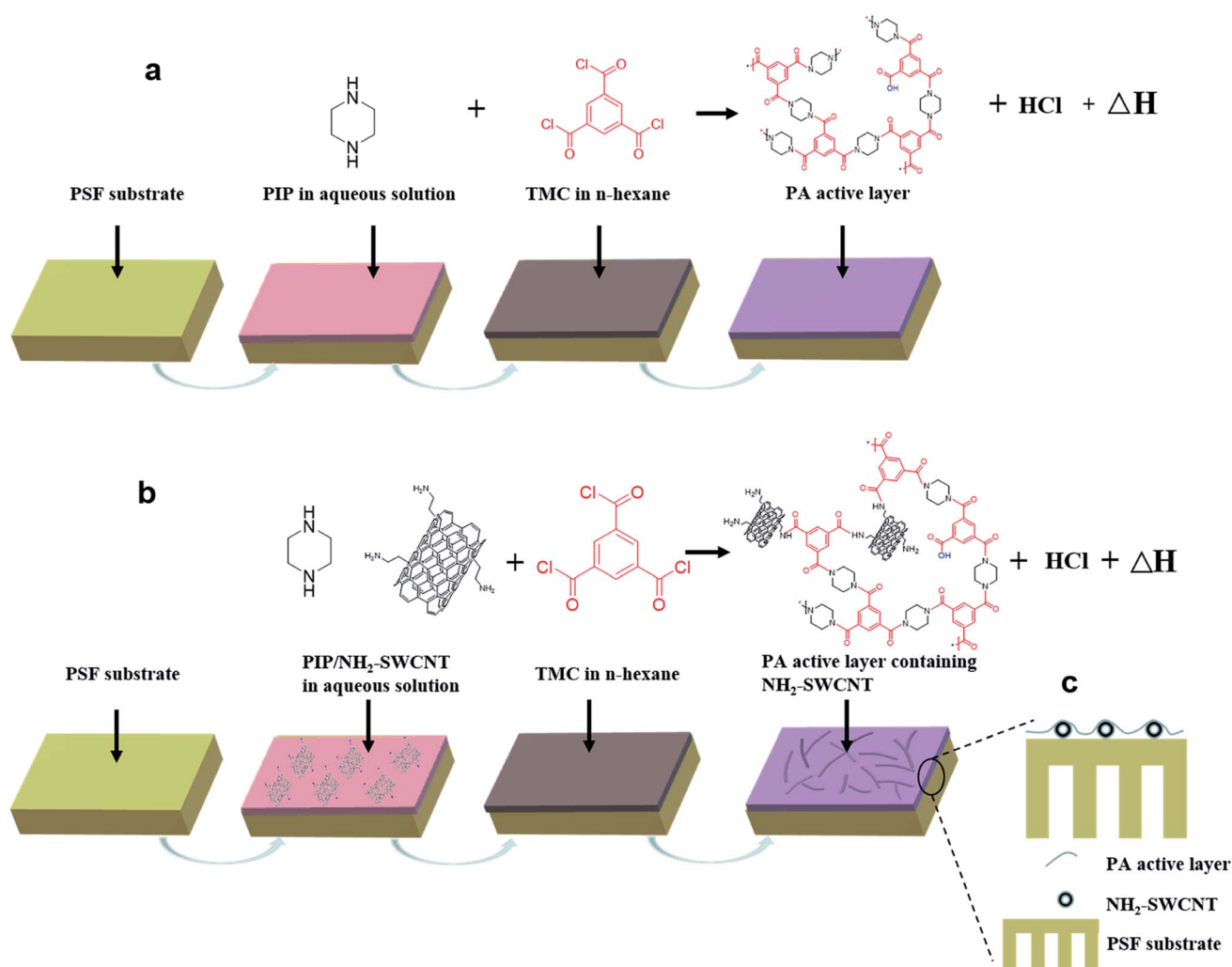

Fig. 1 Schematics of the interfacial polymerization process and the resultant membrane (a) TFC NF membrane. (b) NH_2-SWCNT-TFN membrane. (c) PA active layer containing NH_2-SWCNTs on the PSF surface.

production, NH₂-SWCNT-TFN NF membranes with large effective areas offer more adsorption positions and diffusion channels for water, leading to significant enhancement of water transport. Moreover, thanks to the more integral PA active layer, facilitated by reaction of amino group on NH₂-SWCNT with acyl chloride group on TMC, there was no significant sacrifice of membrane rejection. The results demonstrate that the prepared membranes have significantly improved desalination performance stability and antifouling ability, and can potentially overcome the trade-off between permeability and selectivity at relatively low concentrations and low pressures.

2. Experimental

2.1 Materials

NH₂-SWCNT powder (purity: > 95%, diameter: 1–2 nm, length: 1–3 μm) was obtained from XFNANO Co., Ltd. (Nanjing, China). Piperazine (PIP) hexahydrate (98%), and 1,3,5-benzene-tricarbonyl trichloride (TMC, 98%) were purchased from Aladdin Co., Ltd. (Shanghai, China). *N*-Hexane (purity ≥ 97%)

was supplied by KESHI Co., Ltd. (Chengdu, China). Bovine serum albumin (BSA, M_w = 67.000 g mol^{-1}) were purchased from Sinopharm Co., Ltd. (Shanghai, China). Polysulfone ultrafiltration membranes were used as the support membranes and were purchased from DelStar Technologies Co., Ltd (Suzhou, China).

2.2 Preparation of TFC NF and NH₂-SWCNT-TFN NF membranes *via* IP

The PA layers of the TFC NF membranes were prepared through IP on PSF ultrafiltration membrane. As schematically shown in Fig. 1a, the PSF membrane was first soaked in distilled water for 30 min and then immersed in a PIP aqueous solution (concentrations of 0.25 wt%, 0.5 wt%, 0.75 wt%, and 1 wt%) for 5 min. The excess PIP aqueous solution was then carefully removed by rolling a smooth rod until no droplets were visible on the surface of the PSF membrane. Subsequently, *n*-hexane solution containing 0.038 wt% TMC solution was poured onto the wetted support membrane, which was left to stand for 2 min
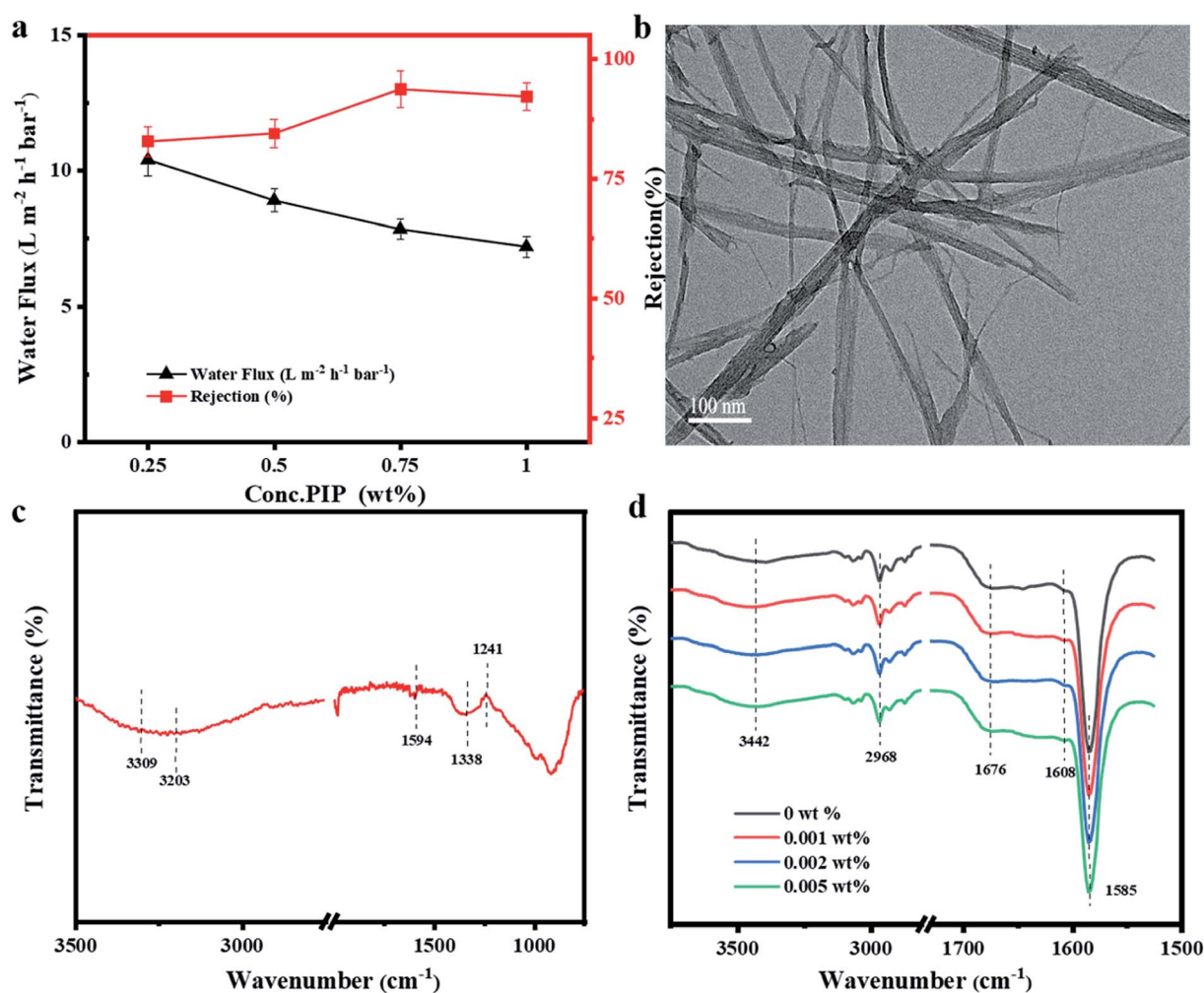

Fig. 2 (a) Pure water flux and MgSO₄ rejection of TFC NF membranes fabricated at different PIP concentrations under pressure of 3.5 bar at room temperature. (b) TEM images of NH₂-SWCNT. (c) FTIR spectra of NH₂-SWCNT in the range of 500–1000 cm^{-1}. (d) FTIR spectra of TFC NF membrane and NH₂-SWCNT-TFN membranes.

to allow the IP reaction to occur. Finally, after the excess TMC/n-hexane solution was poured out, the membrane was rinsed with n-hexane and immediately heated at 80 °C for 3 min to obtain

a well-formed PA separation layer. The NH$_2$-SWCNT-TFN NF membrane was prepared in the same way as the TFC NF membrane with the only difference being that the aqueous
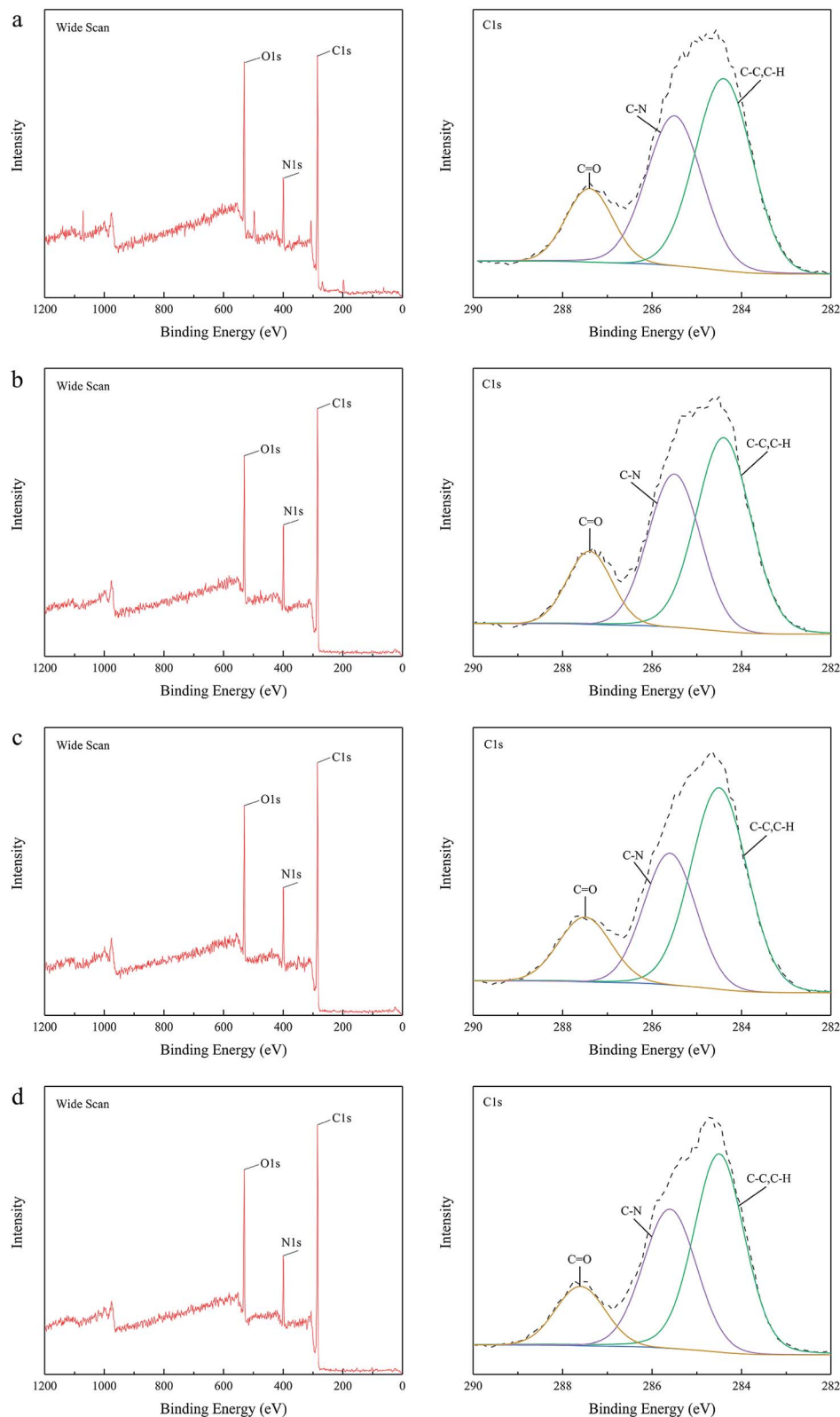

Fig. 3 XPS wide-scan and C 1s core level of (a) TFC, (b) NH$_2$-SWCNT-0.001 wt%, (c) NH$_2$-SWCNT-0.002 wt%, (d) NH$_2$-SWCNT-0.005 wt%.

solutions in the case of the former contained 0.75 wt% (optimum concentration) of PIP and NH_2-SWCNT in varying concentrations (0.001 wt%, 0.002 wt%, and 0.005 wt%), which were well dispersed by sonication (Fig. 1b). All membranes were prepared in a fume hood at room temperature.

2.3 Characterisation methods

Transmission electron microscopy (TEM) was utilised to observe the morphologies of the NH_2-SWCNTs while Fourier transform infrared spectroscopy (FTIR) was applied to characterise their chemical structures. The membrane surface morphologies were analysed using scanning electron microscopy (SEM) while membrane surface roughness were analysed *via* atomic force microscopy (AFM). Attenuated total reflectance-FTIR spectroscopy (ATR-FTIR) and X-ray photoelectron spectroscopy (XPS) were employed separately to investigate the functional chemical structures and chemical compositions of the top surfaces of the prepared membranes. Hydrophilicity of the membrane surfaces was evaluated through water contact angle instrument (JC2000C2, POWEREACH, China) and the equilibrium contact angle reported. Further, the zeta potential of each membrane surface was measured using a zeta potential analyser (EKA, Anton Paar GmbH, Austria), and the pH values were in the range 3–9.

2.4 Separation performance of membranes

A cross-flow membrane filtration apparatus with an effective area of 36 cm² was used to test the separation performances of the membranes at low operating pressure of 3.5 bar and room temperature. $MgSO_4$ and Na_2SO_4 solutions (2000 ppm) were used to investigate the rejection of the prepared membranes, respectively. Rejection was measured based on the conductivities of both the feed and permeate solutions using the following equation:

$$R_j = (1 - C_p/C_f) \times 100\% \tag{1}$$

Here, C_p is conductivity of the filtrate solution, and C_f is conductivity of the initial feed solution.

The following formula was used to calculate the pure water flux of the membranes prepared.

$$J = V/(A \times t) \tag{2}$$

Here, J is permeate flux (L m⁻² h⁻¹ bar⁻¹), V is volume of permeate (L), A is effective area (m²), and t is time interval (h).

2.5 Evaluation of antifouling property of membranes prepared

A series of cross-flow membrane filtration tests was employed to evaluate the surface fouling of the prepared membranes *via* measurement of the amounts of protein adsorbed by the membranes during filtration. All the experiments were operated at a pressure of 3.5 bar and room temperature. The model protein, BSA, was dissolved in a 2000 ppm Na_2SO_4 solution at a concentration of 500 mg L⁻¹ to serve as the feed solution. The

flux of the feed solution was measured based on the amount of water permeated through the membranes. The BSA rejections of the membranes prepared were evaluated according to eqn (1), where C_p and C_f were the BSA contents of the penetrating and feed solutions which measured by the BSA absorption on membranes, respectively. Firstly, pure water was filtered for 40 min and the data were recorded every 5 min. Then, the BSA/Na_2SO_4 solution was substituted for the feed solution and the data were recorded. The pure water flux was recorded again after 40 min of testing and 5 min of flushing. The flux recovery ratio, FRR, was calculated as follows:

$$\text{FRR } (\%) = J_2/J_1 \times 100\% \tag{3}$$

Here, J_1 and J_2 are the fluxes of initial pure water and pure water in the third step of the antifouling experiment, respectively.

3. Results and discussion

3.1 Selection of best formulation of TFC NF membrane

A cross-flow permeation test was employed to measure the membrane performance in terms of water flux and salt rejection. Fig. 2a illustrates the water flux and salt rejection rates of the bare NF membranes for various concentrations of PIP monomer; these investigations were carried out to determine the optimum formulation. With decrease in PIP contents from 1 wt% to 0.25 wt%, the water flux evidently increased from 7.84 L m⁻² h⁻¹ bar⁻¹ to 10.4 L m⁻² h⁻¹ bar⁻¹. This change arises principally from the combined actions of the decreased PA thickness, hydrophilicity, and surface roughness.[37] However, as is shown, despite the increase in membrane water flux, the rejection rate of $MgSO_4$ decreased evidently. The rejection rate was at satisfactory levels only at concentrations of 1 wt% and 0.75 wt%. Both flux and rejection rate increased with decrease in PIP content from 1 wt% to 0.75 wt%, which can be attributed to the membrane surface becoming more negatively charged and the emergence of a powerful repulsive force to the negatively charged anions, bringing about better selectivity. Besides, high water flux can help dilute the filtrate and thus enhance salt rejection.[10] Consequently, the optimum PIP concentration was 0.75 wt%, and hence this formulation was chosen for the addition of NH_2-SWCNTs to further improve the NF performance.

3.2 Characterisation of NH_2-SWCNTs

The morphologies of the NH_2-SWCNTs are illustrated in Fig. 2b. The hollow cylindrical nanostructures of the NH_2-SWCNTs were

Table 1 XPS data of the TFC NF membranes and NH_2-SWCNT-TFN membranes

Sample	C 1s content (%)	N 1s content (%)	O 1s content (%)
TFC	61.54	17.19	21.27
TFN-0.001 wt%	62.54	17.97	19.48
TFN-0.002 wt%	64.55	17.63	17.82
TFN-0.005 wt%	61.83	18.24	19.94

distinctly observed in these TEM images and the lengths of the NH$_2$-SWCNTs were especially low. The functional groups and chemical bonding of the NH$_2$-SWCNTs were analysed via ATR-FTIR, as shown in Fig. 2c. In the spectrum, the absorption frequency at 1594 cm^{-1} is related to the stretching vibrations of

the C=C aromatic bonds attached to the NH$_2$-SWCNT structures.[38] The peak of the C–N grafted amide bond was observed at 1241 cm^{-1}. The stretching vibrations of the second amide N–H manifested a square-shaped band in the range 3400–3500 cm^{-1}, and the tensile variations of the aromatic primary
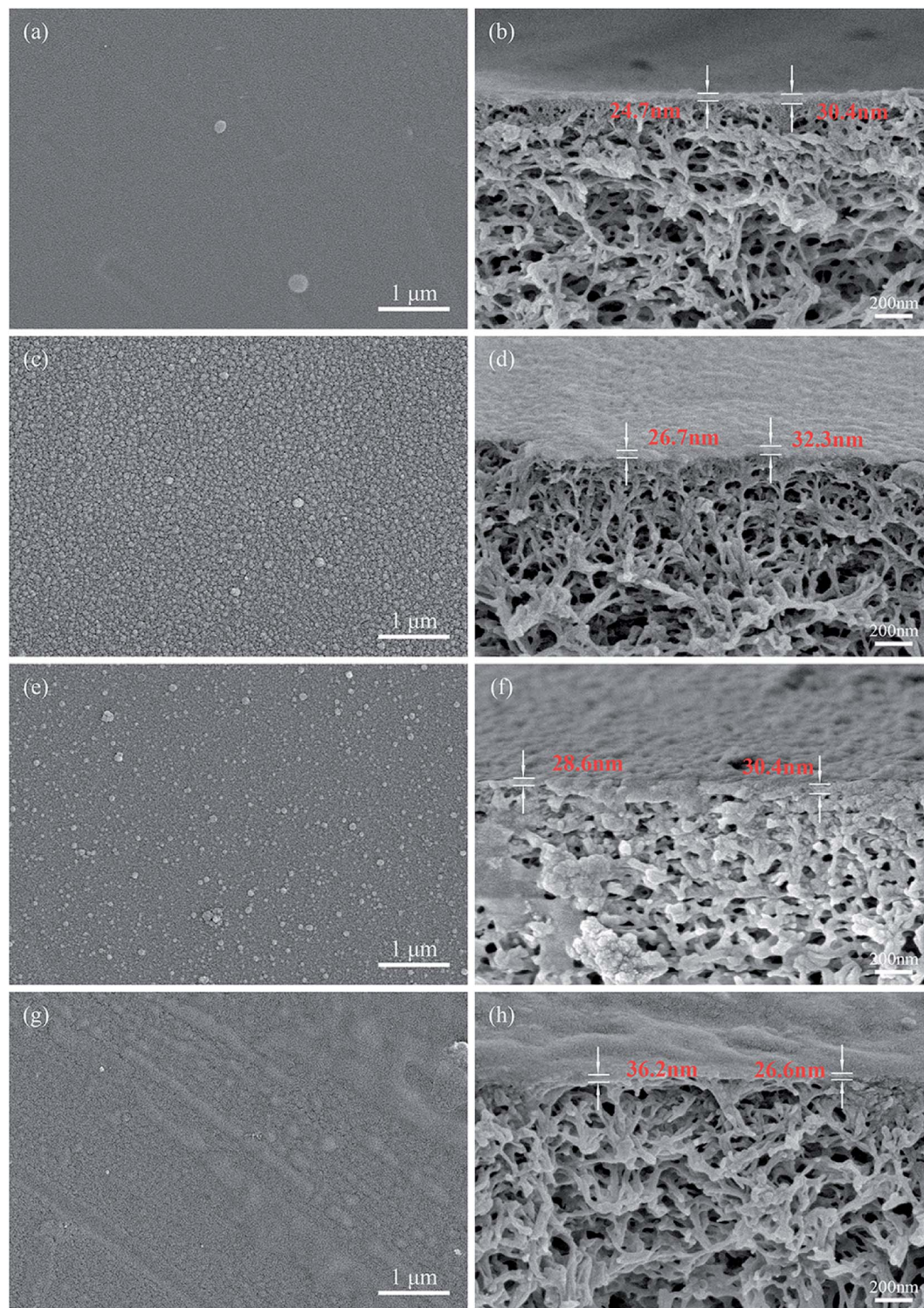

Fig. 4 SEM images of top surfaces and cross-sections of (a and b) TFC, (c and d) NH$_2$-SWCNT-0.001 wt%, (e and f) NH$_2$-SWCNT-0.002 wt%, (g and h) NH$_2$-SWCNT-0.005 wt%.

amine N–H resulted in two wide bands in the frequency regions 3200–3300 cm^{-1} and 3300–3350 cm^{-1}. Accordingly, the stretching variations of the amine N–H groups and amide N–H overlap to a certain extent.[39] It can be concluded that aromatic diamines are connected to the surface of the SWCNTs through the amide bond at one end such that the other end of the diamines is maintained as a free amino group.

3.3 Characterisation of NH₂-SWCNT-TFN membranes

3.3.1 Surface chemical compositions of NH₂-SWCNT-TFN membranes. The ATR-FTIR spectra of the pristine and NH₂-SWCNT-TFN membranes are illustrated in Fig. 2d. The characteristic peaks for fully aromatic polyamide are 1608 cm^{-1}, which were attributed to C=O stretch vibrations of the amide groups, validated that the IP between PIP and TMC was successful.[40] Although the ATR-FTIR spectra of the NH₂-SWCNT-TFN membranes did not present the NH₂-SWCNT peaks owing to low concentration, the darker colour of the membrane surfaces demonstrated the existence of NH₂-SWCNTs in the PA active layer. Furthermore, XPS analysis was employed to verify the crosslinking variation and incorporation of NH₂-SWCNTs into the TFC NF membranes. As displayed in Fig. 3, all the membranes had three peaks at binding energies of

284.8 eV, 399.6 eV, and 531.0 eV, representing the C 1s, N 1s, and O 1s regions, respectively. Table 1 shows that the NH₂-SWCNT-TFN membranes possessed slightly higher N contents and lower O contents. In addition, the embedment of NH₂-SWCNTs into the TFC NF membranes slightly increased their contents of C, thereby indicating the potential for interaction between the functional groups of NH₂-SWCNTs and PA chains. NH₂-SWCNT-0.002 wt%-TFN membrane possessed the highest C content and lowest N content, demonstrating the optimal interaction between the functional groups of NH₂-SWCNTs and PA chains, which is in accordance with the optimal performance.

3.3.2 Surface morphologies of NH₂-SWCNT-TFN membranes. The surface morphologies of the TFC NF and NH₂-SWCNT-TFN membranes were analysed via SEM (Fig. 4). All membranes showed a typical nodular surface structure, which is a common feature of IP TFC NF membranes and is principally caused by the cross-linking of active monomers.[41] As shown in Fig. 4a, at low monomer concentrations, the level of HCl and/or the amount of heat was reduced, extremely small nanobubbles were generated, and the nodular surface morphologies of the TFC NF membranes were formed.[42] According to previous theories, the size of the protuberances
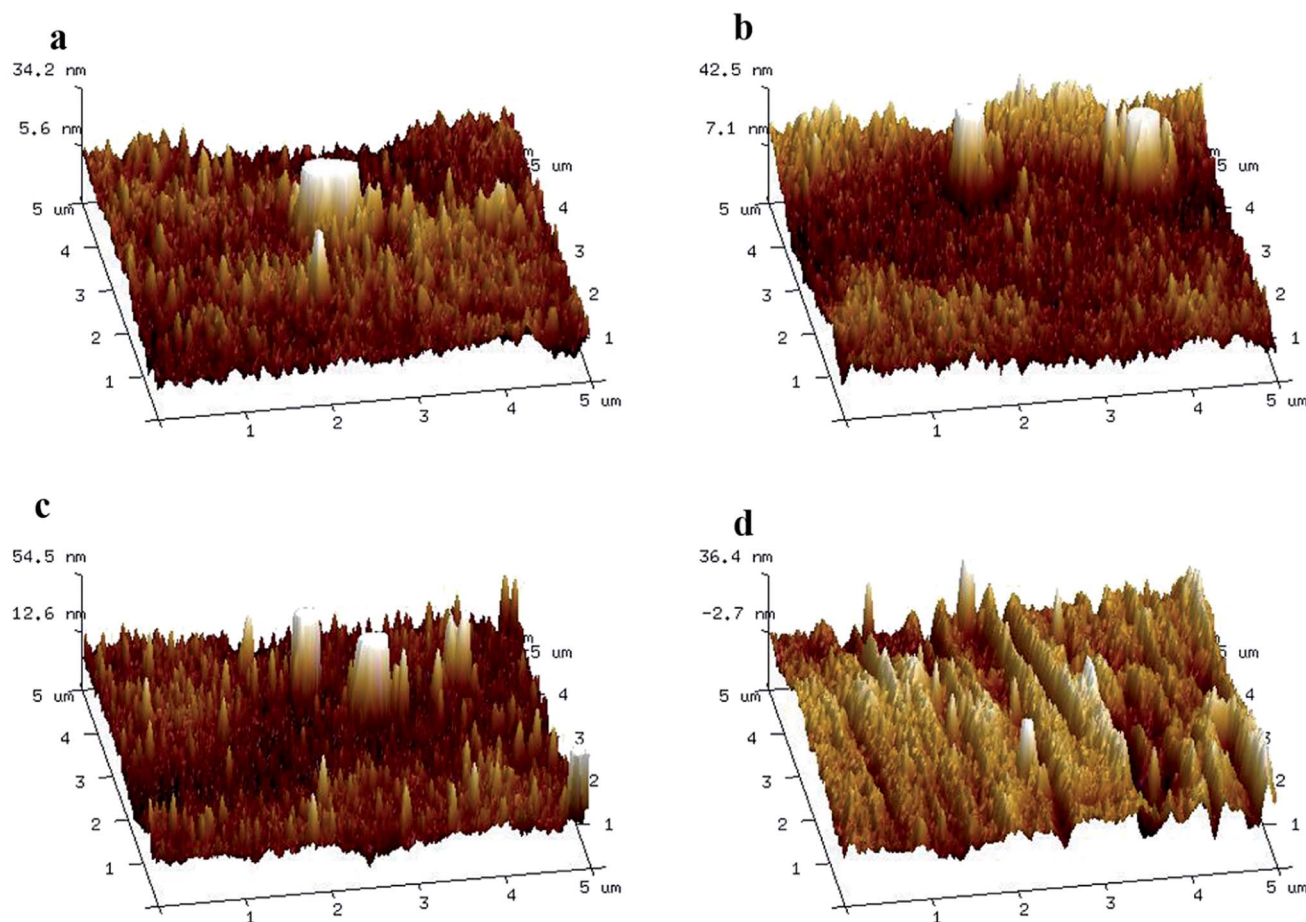

Fig. 5 AFM images of TFC NF and NH₂-SWCNT-TFN membranes (a) TFC, (b) NH₂-SWCNT-0.001 wt%, (c) NH₂-SWCNT-0.002 wt%, (d) NH₂-SWCNT-0.005 wt%.

depends on the initial concentration of the reagent near the initial PA oligomer cluster and the reaction rate between PIP and TMC.[27] The NH_2-SWCNT is hydrophilic and can potentially attract the PIP monomer. When the contents of the embedded NH_2-SWCNTs was 0.001 wt%, the hydrophilicity improved and the local monomer concentration around the NH_2-SWCNTs could be augmented to promote the formation of more, larger, and more distinguishable PA protuberances on the membrane surface, indicating the positive effect of NH_2-SWCNTs in facilitating the IP process. When the concentration of NH_2-SWCNTs was increased to 0.002 wt%, tubular nanobridges emerged between the protuberances, as presented in Fig. 4e. These tubular nanobridges could be attributed to the optimal reaction between the amino group on NH_2-SWCNTs and acyl chloride group on TMC. For the two NH_2 sources, and the lower reaction rate of NH_2-SWCNTs with TMC than that with PIP additionally contributed to this rare phenomenon.[43] When the NH_2-SWCNT content was increased to 0.005 wt%, the SEM image shows that more obvious tubular crumpled structures appeared, which could be ascribed to the characteristic structure of CNTs, while the contour of the nodular structure was covered with a thin PA layer. As the concentration increased, more NH_2-SWCNTs in the aqueous PIP would participate in the IP reaction, leading to the formation of the distinct tubular wrinkles on the surface of active layer. Fig. 4 additionally illustrates the cross-section SEM images of the TFC NF and NH_2-SWCNT-TFN membranes. Both membranes exhibited an ultra-thin dense active layer, about
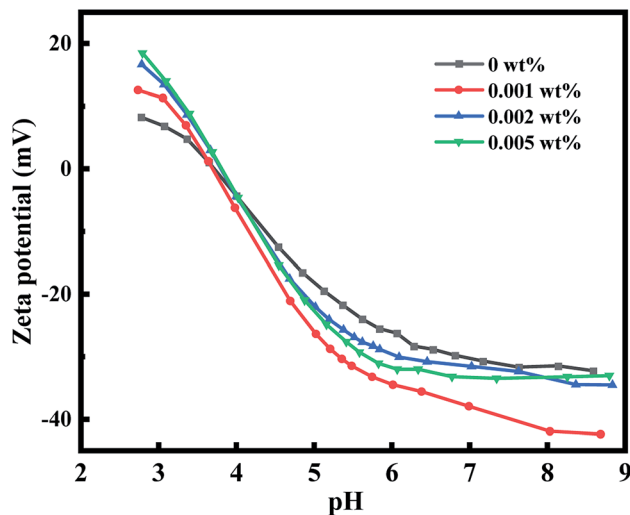

Fig. 7 Surface zeta potential under different pH for NH_2-SWCNT-TFN membranes.

30 nm thick, as a result of the decreasing IP reaction rate at lower monomer concentrations.[10] Moreover, the NH_2-SWCNTs had a negative impact of retarding monomer diffusion, rendering it harder for PIP to penetrate the active layer during IP reaction, which restricted the extension of the active layer.

To further study the surface morphologies, AFM images, 5 µm × 5 µm in area, were analysed (Fig. 5). In the fabrication of
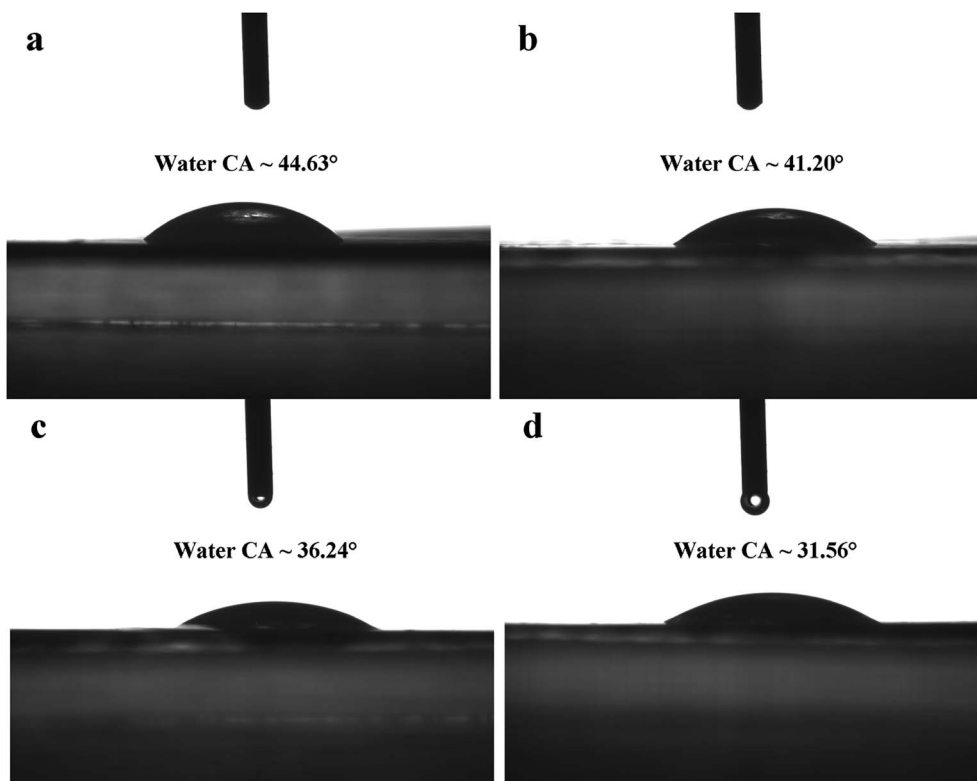

Fig. 6 Water contact angles of TFC NF and NH_2-SWCNT-TFN membranes (a) TFC, (b) NH_2-SWCNT-0.001 wt%, (c) NH_2-SWCNT-0.002 wt%, (d) NH_2-SWCNT-0.005 wt%.

TFC NF membranes, PIP easily penetrated the interface between the aqueous and organic phases owing to its low molecular weight, yielding thicker and smoother top surfaces of the PA active layers. In the case of the NH_2-SWCNT-TFN membranes, PIP was likely to encounter more resistance to diffusion across the interface of NH_2-SWCNTs, which rendered the fabricated active layer thinner and rougher. However, when the concentration was increased further to 0.005 wt%, NH_2-SWCNT agglomerated to some extent and the surface roughness began to decline, which possibly indicates that the hindering impact of NH_2-SWCNT on PA formation becomes dominant when the NH_2-SWCNT content exceeds a certain level. Generally, differences between the diffusion coefficients of the activator and inhibitor,[44] and the hydrophilicity and viscosity of NH_2-SWCNTs act collectively in the fabrication of TFN NF membranes.

3.3.3 Water contact angle and zeta potential measurements. The water contact angles (Fig. 6) were measured to evaluate the hydrophilicity of the membranes prepared. The contact angle gradually decreased from 44.63° to 31.56° with increase in concentration of NH_2-SWCNTs, indicating that the hydrophilic NH_2-SWCNTs were incorporated into the surfaces of the membranes prepared, rendering them more hydrophilic. The decline in water contact angle can be attributed to the increased roughness, along with the tubular structure of NH_2-SWCNT and hydrophilicity of amine groups.[45] It is proposed that water was partly transported through the tunnel of NH_2-SWCNT and was consequently attached to the inner and external surfaces of the tunnel, which reduced the water contact angle.

Fig. 7 shows the surface zeta potential of the active layer under different pH, which exerts significant influence on solute rejection. As shown, all the membranes prepared presented negatively charged surfaces in the pH range 3.5–9, and these surfaces became more negatively charged with an increase in
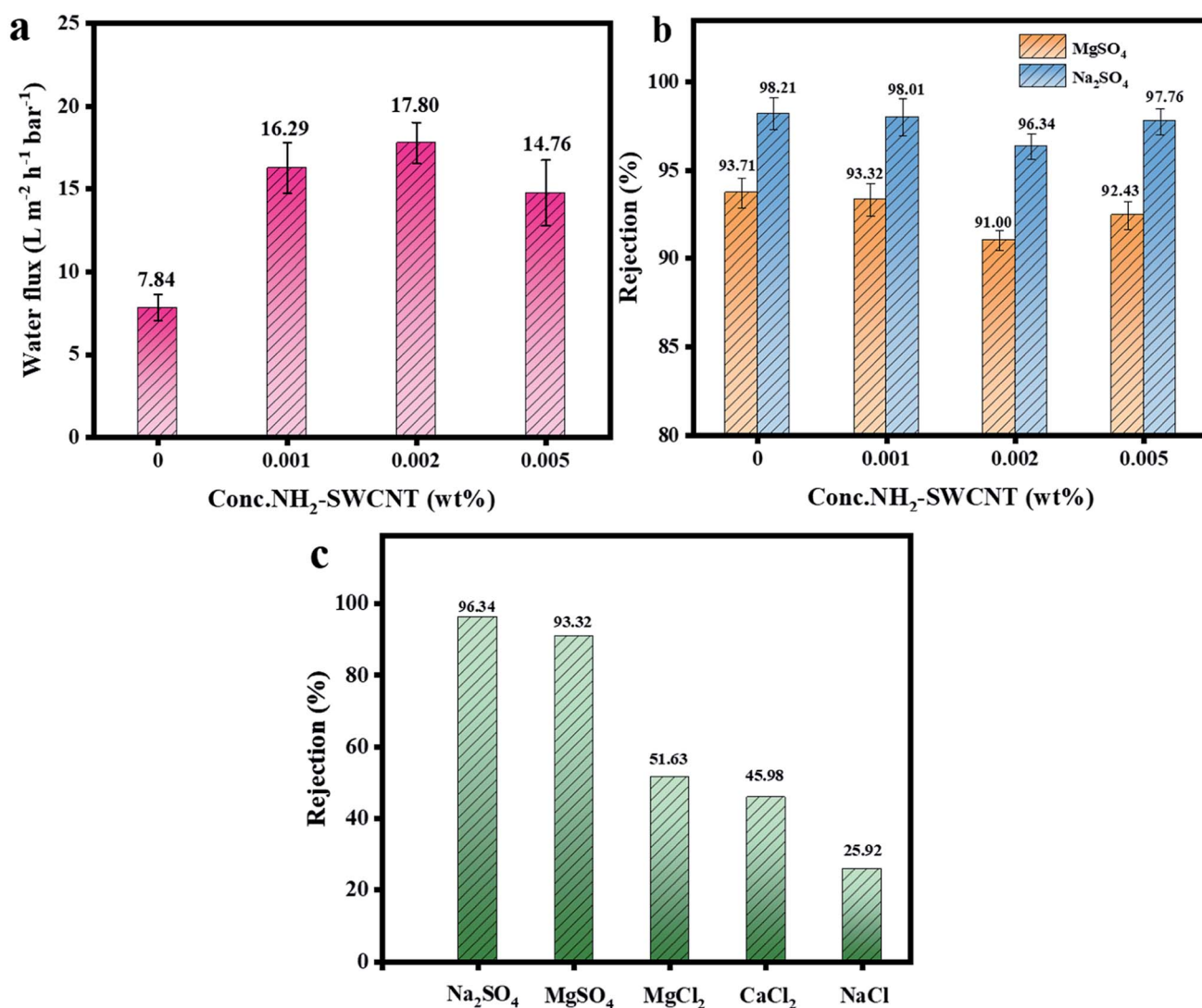

Fig. 8 (a) Pure water flux. (b) Salt (2000 ppm Na_2SO_4 and $MgSO_4$, respectively) rejection of the TFC NF and NH_2-SWCNT-TFN membranes at 0.75 wt% PIP concentration with different NH_2-SWCNT amounts under pressure of 3.5 bar, respectively. (c) The rejection of different kinds of salts (2000 ppm, respectively) of the NH_2-SWCNT-0.002 wt%-TFN membrane.

NH_2-SWCNT concentration, thereby validating the successful embedment of NH_2-SWCNTs into the PA active layers. In general, the protonation of amine groups leads to positive charge of the membrane at low pH values, while the deprotonation of carboxylic acid groups leads to negative charge at high pH values.[10] In the case of TFC NF membranes without embedded NH_2-SWCNTs, the carboxylic acid groups mainly originate from TMC, while groups containing N exist in the PIP monomer and are generally unreacted amine groups.[46] In the case of the NH_2-SWCNT TFN membranes, NH_2-SWCNT has both unreacted carboxylic and amine groups in its nanotube structure, causing increased contribution to negative charges on the membrane surfaces. Based on the Donnan effect, PA active layers with stronger negative zeta potentials reject divalent ions more successfully.[47]

3.4 Separation performance NH_2-SWCNT-TFN membrane

Fig. 8a illustrates the pure water flux and salt rejection rates of the TFC NF and NH_2-SWCNT-TFN membranes. In all membranes, the water flux increased significantly with the incorporation of NH_2-SWCNTs at different concentrations. The enhancements of flux and permeance were attributed to the following factors. Firstly, the ultra-thin PA active layer remarkably decreased the distance of, and resistance to the passage of water, and hence improved water permeation. Secondly, both the internal voids of the NH_2-SWCNT tubular structure and the additional water passages formed by the interspaces between the PA chains and NH_2-SWCNTs promoted the water flux of the prepared membranes.[25] Besides, the weak carbon–water interactions on the surfaces of the smooth NH_2-SWCNTs promoted water transport.[48] At low pressures, the weak carbon–water interactions played a dominant role as the inner nanochannels were too thin for water transport. Thirdly, the rougher and more
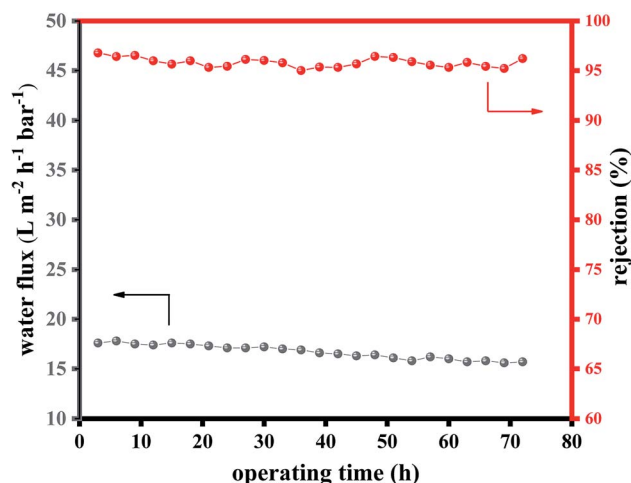

Fig. 9 Long-term cross-flow filtration test of the NH_2-SWCNT-0.002 wt%-TFN membrane over 72 hours (3.5 bar, room temperature, 2000 ppm of Na_2SO_4).

hydrophilic surfaces further enhanced water flux. As established from the AFM images, the incorporation of NH_2-SWCNTs helped increase the roughness of the TFC NF membranes, thereby enlarging the surface areas available for water transport. Furthermore, the enhanced hydrophilicity of the NH_2-SWCNT-TFN membranes was beneficial to the adsorption of water molecules, thereby effectively increasing water permeation.[49] When the concentration of NH_2-SWCNT increased from 0 wt% to 0.002 wt%, the water flux improved from 7.2 L m^{-2} h^{-1} bar^{-1} to 17.8 L m^{-2} h^{-1} bar^{-1}, and decreased slightly thereafter. This was attributed to the reduction in membrane roughness and agglomeration of NH_2-SWCNTs in higher quantities despite the increase in hydrophilicity. Meanwhile, the best interaction between the functional groups of NH_2-SWCNTs and PA chains

Table 2 Comparison with commercial NF membranes and various NF membranes reported in literature containing different nanomaterials at their optimized concentration

Membrane	Additive	Flux (L m^{-2} h^{-1} bar^{-1})	Rejection (%, Na_2SO_4)	Thickness of PA layer (nm)	Operating pressure (bar)	Reference
NF270	Bare	11.14	98.4		6	Measured
NF90	Bare	9.51	98.6		28	Measured
TFN NF	SGO	2.37	96.45	113.8 ± 2.9	5	51
Poly(piperazine-amide) NF	rGO/TiO2	6.1	94	600	10	52
TFN NF	GO	15.63	96.56	27–35	4	10
TFC NF	Tannic acid/Fe^{3+} nanoscaffold	19.6	95.0 ± 1.0	54.9 ± 1.8	5.7 ± 1.0	17
TFN NF	PDA/PEG nanocapsule	11.7	95	120–135	2–5	53
TFC NF	Cellulose nanocrystals	34	97	~100	6	54
Nanocomposite NF	Oxidized MWCNT	2.3	85		4	28
TFC NF	NH_2-MWCNT	5.1	95.72		10	29
Ultrathin TFC PA NF	CNT	23.7	46.5	31.1 ± 5.6	10	30
TFN NF	TA-MWCNT	31.4	56		6	31
TFN NF	Aluminosilicate SWCNT	<1.2	97		10	32
Nanocomposite NF	MWCNT-OH	6.9	97.6	77	6	
	MWCNT-COOH	6.2	96.6	84	6	27
	MWCNT-NH	5.3	96.8	71	6	
TFN NF	PMMA-MWNT	7	99		10	33
TFN NF	Sulfonated MWCNT	13.2	96.8	100–150	6	34
TFN NF	NH_2-SWCNT	17.8	96.34	30 ± 3.3	3.5	This work

and the unique tubular nanobridges structure of the NH$_2$-SWCNT-0.002 wt%-TFN membrane provided the largest surface area and maximum roughness, which further enhanced flux.

Fig. 8b presents the salt rejection rates of the prepared membranes. In the case of Na$_2$SO$_4$, the rejection rate slightly decreased from 98.21% to 96.34% with the addition of NH$_2$-SWCNTs and then mildly improved when the NH$_2$-SWCNT concentration was 0.002 wt%, but remained lower than those of the TFC NF membranes. The trade-off between permeability and solute selectivity leads to the reduction in salt rejection rate in the context of improved water flux. For one thing, a thinner active layer can partially lose the capacity to select solutes. In addition, the selectivity-limited water channel of NH$_2$-SWCNTs and potential voids in the PA active layers contribute to the decline in salt rejection rate. For another thing, as the NH$_2$-SWCNT content increases, the adhesion of the terminal amino group on NH$_2$-SWCNT and the PA chain becomes tighter, which could improve

the rejection ability. Besides, the viscosity of the mixed solution during IP reaction increased with the higher NH$_2$-SWCNT content, whereby the out-diffusion of the solvent from the cast solution is preferred to the in-diffusion of the non-solvent into the solution, resulting in the formation of smaller pores in the microporous membrane, which would be beneficial for a higher salt rejection.[24,50] Under the combined effects of the above factors, although the trade-off was not completely eliminated, it was reduced to such a low level that the retention rate changed little. The rejection of different salts followed the sequence of Na$_2$SO$_4$ > MgSO$_4$ > MgCl$_2$ > CaCl$_2$ > NaCl (Fig. 8c), which confirms that the ion sieving mechanism of the membrane is a synergistic effect of strong Donnan exclusion size sieving.[11]

To have a better evaluation of the general desalination performance of NF membrane, Table 2 compares the water flux, salt rejection and operating pressure of membranes prepared in this work, commercial membranes, and various NF membranes
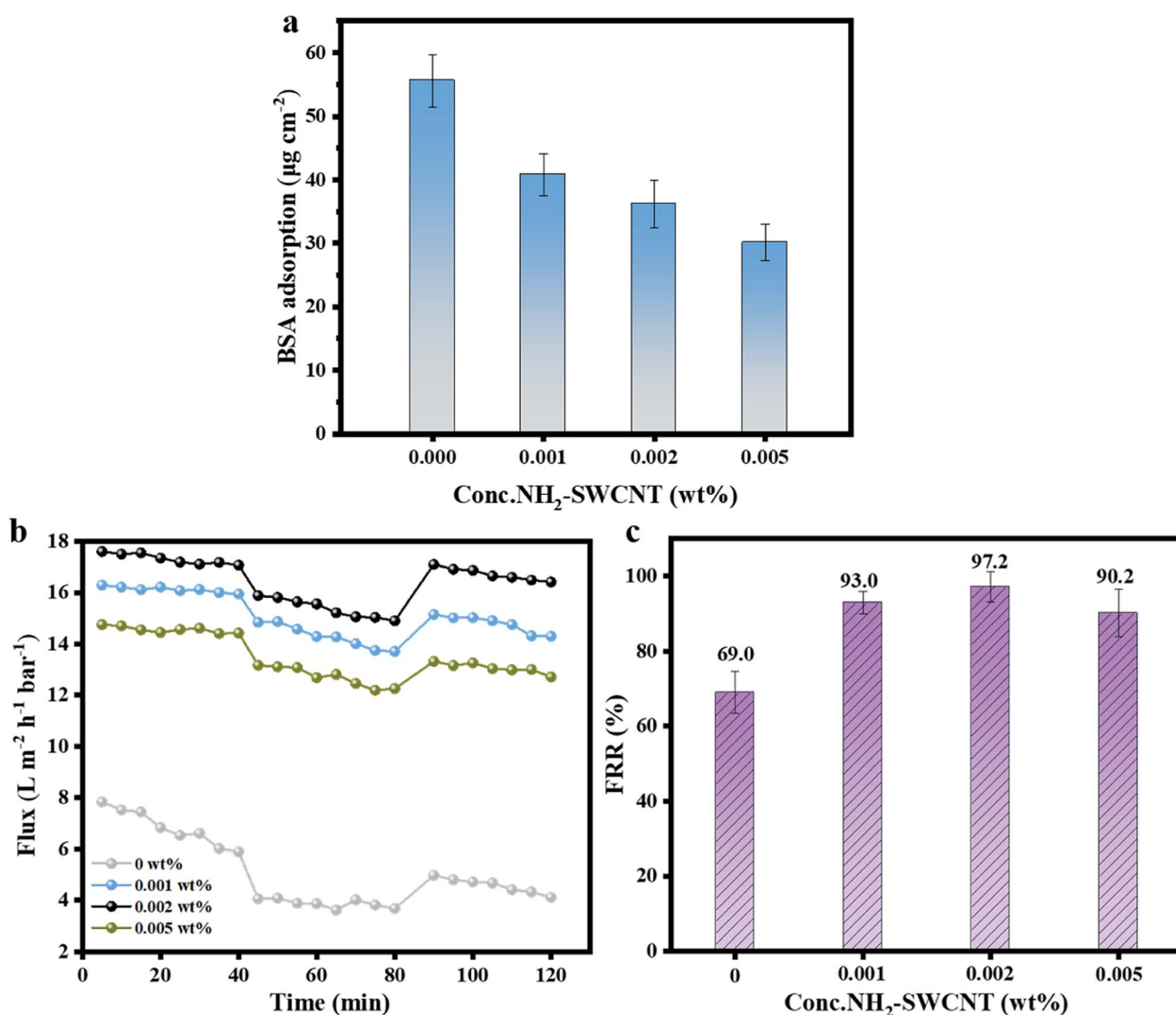

Fig. 10 (a) The amount of BSA adsorbed on prepared membranes. (b) Flux *versus* time for TFC NF and NH$_2$-SWCNT-TFN membranes at 3.5 bar during three stages: pure water flux for 40 min, BSA/NA$_2$SO$_4$ solutions flux for 40 min, and water flux after 5 min washing with pure water. (c) Flux recovery ratio (FRR) of TFC NF and NH$_2$-SWCNT-TFN membranes after BSA fouling.

reported in literature containing different nanomaterials especially different CNT-polymer composites. It is clearly seen from the table that the performance parameters for the NH_2-SWCNT-TFN membrane were superior to most reported CNT-polymer composite membranes thanks to NH_2-SWCNT incorporated in interfacial polymerization.

3.5 Long-term stability of NH_2-SWCNT membrane

Operational stability is an essential parameter for the practical industrial application of the NF. A long-term NF test was conducted with water flux and Na_2SO_4 rejection recorded for 72 hours to investigate the performance stability of NH_2-SWCNT-0.002 wt%-TFN membrane. As illustrated in Fig. 9, NH_2-SWCNT-0.002 wt%-TFN membrane had insignificant fluctuation in flux and rejection indicating that the high performance of the prepared membrane is stable over time, which could further demonstrate that the adhesion of the terminal amino group on –NH to the PA chain is tight. The slightly decreased permeability and increased rejection over time can be attributed to membrane compaction.[30]

3.6 Evaluation antifouling property

Fouling is a noticeable drawback that can lead to decreased flux and shortened the lifetime of membranes. It is critical to investigate the antifouling performance of the membranes. Fig. 10a shows the BSA adsorption decreased thanks to the hydrophilicity improved by the incorporation of hydrophilic groups of NH_2-SWCNT. Meanwhile, Fig. 10b shows the flux variations of the membranes during three stages. As illustrated, although the flux values of the NH_2-SWCNT-TFN membranes presented a tendency to decline, the extent of decline was evidently lower than that in bare TFC NF membranes. To further evaluate the antifouling property of the membranes, FRR was measured. As seen in Fig. 10c, the bare TFC NF membranes exhibited the least FRR value of 69.0%, while the NH_2-SWCNT-TFN membranes showed higher FRR value of up to 97.2%. The excellent test results of the NH_2-SWCNT-TFN membranes indicated that incorporating NH_2-SWCNTs dramatically improved antifouling property compared to TFC membrane which showed significant irreversible fouling. The NH_2-SWCNTs contributed to the enhancement of antifouling ability and possessed zwitterionic groups, thereby carrying both positive and negative charges, and thus produced strong and stable electrostatic interactions with water.[12] Furthermore, embedding NH_2-SWCNTs improved the coverage fraction of hydrophilic groups on the membrane surfaces.[35] These two factors resulted in the formation of a denser hydration layer, which made it difficult for fouling to blend with the membrane surface, and hence fouling was reduced, and membrane recovery was easier. In addition to good antifouling ability, the enhancement of stability was evident.

4. Conclusion

A novel TFN NF membrane was fabricated on a PSF ultrafiltration membrane *via* an IP technique with PIP/NH_2-SWCNT and TMC

serving as the aqueous and organic phase monomers, respectively. By incorporating low contents of NH_2-SWCNTs at low monomer concentrations, a series of ultra-thin integral PA active layers with irregular structure and improved hydrophilicity, roughness, and surface charge was formed. Meanwhile, owing to the unique characteristics of NH_2-SWCNTs, including their distinctive water channels and the role of N–H groups, the NH_2-SWCNT-TFN membranes with tubular nanobridges presented improved permeability that rarely compromised salt rejection ability. At the optimum formulation condition (0.75 wt% PIP and 0.038 wt% TMC), the NH_2-SWCNT-0.002 wt%-TFN membrane exhibited the maximum water flux of 17.8 L m^{-2} h^{-1} bar^{-1} with Na_2SO_4 rejection of 96.34% and $MgSO_4$ rejection of 91.0%. Moreover, the NH_2-SWCNT-TFN membranes exhibited improved stability and antifouling property. Overall, this strategy can be used to effectively overcome the trade-off phenomenon and provides a method for fabricating scalable high-performance ultra-thin TFN NF membranes (operating under a low pressure of 3.5 bar) for nanofiltration.

Conflicts of interest

There are no conflicts to declare.

Acknowledgements

References

1 M. M. Mekonnen and A. Y. Hoekstra, Four billion people facing severe water scarcity, *Adv. Sci.*, 2016, **2**, e1500323, DOI: 10.1126/sciadv.1500323.

2 M. A. Shannon, P. W. Bohn, M. Elimelech, J. G. Georgiadis, B. J. Mariñas and A. M. Mayes, Science and technology for water purification in the coming decades, *Nature*, 2009, **452**, 337–356, DOI: 10.1142/9789814287005_0035.

3 R. J. Petersen, Composite reverse osmosis and nanofiltration membranes, *J. Membr. Sci.*, 1993, **83**, 81–150, DOI: 10.1016/0376-7388(93)80014-o.

4 R. Xu, J. Wang, D. Chen, T. Liu, Z. Zheng, F. Yang, J. Chen, J. Kang, Y. Cao and M. Xiang, Preparation and performance of a charge-mosaic nanofiltration membrane with novel salt concentration sensitivity for the separation of salts and dyes, *J. Membr. Sci.*, 2020, **595**, 117472, DOI: 10.1016/j.memsci.2019.117472.

5 Y. Zhu, W. Xie, S. Gao, F. Zhang, W. Zhang, Z. Liu and J. Jin, Single-Walled Carbon Nanotube Film Supported Nanofiltration Membrane with a Nearly 10 nm Thick

Polyamide Selective Layer for High-Flux and High-Rejection Desalination, *Small*, 2016, **12**, 5034–5041, DOI: 10.1002/smll.201601253.

6 M. M. Pendergast and E. M. V. Hoek, A review of water treatment membrane nanotechnologies, *Energy Environ. Sci.*, 2011, **4**, 1946–1971, DOI: 10.1039/c0ee00541j.

7 S. J. Gao, H. Qin, P. Liu and J. Jin, SWCNT-intercalated GO ultrathin films for ultrafast separation of molecules, *J. Mater. Chem. A*, 2015, **3**, 6649–6654, DOI: 10.1039/c5ta00366k.

8 M. Guo, S. Wang, K. Gu, X. Song, Y. Zhou and C. Gao, Gradient cross-linked structure: towards superior PVA nanofiltration membrane performance, *J. Membr. Sci.*, 2019, **569**, 83–90, DOI: 10.1016/j.memsci.2018.10.006.

9 Y. Han, Z. Xu and C. Gao, Ultrathin Graphene Nanofiltration Membrane for Water Purification, *Adv. Funct. Mater.*, 2013, **23**, 3693–3700, DOI: 10.1002/adfm.201202601.

10 W. Zhao, H. Liu, N. Meng, M. Jian, H. Wang and X. Zhang, Graphene oxide incorporated thin film nanocomposite membrane at low concentration monomers, *J. Membr. Sci.*, 2018, **565**, 380–389, DOI: 10.1016/j.memsci.2018.08.047.

11 Z. Wang, Z. Wang, S. Lin, H. Jin, S. Gao, Y. Zhu and J. Jin, Nanoparticle-templated nanofiltration membranes for ultrahigh performance desalination, *Nat. Commun.*, 2018, **9**, 1–9, DOI: 10.1038/s41467-018-04467-3.

12 W.-F. Chan, E. Marand and S. M. Martin, Novel zwitterion functionalized carbon nanotube nanocomposite membranes for improved RO performance and surface anti-biofouling resistance, *J. Membr. Sci.*, 2016, **509**, 125–137, DOI: 10.1016/j.memsci.2016.02.014.

13 R. Hu, R. Zhang, Y. He, G. Zhao and H. Zhu, Graphene oxide-in-polymer nanofiltration membranes with enhanced permeability by interfacial polymerization, *J. Membr. Sci.*, 2018, **564**, 813–819, DOI: 10.1016/j.memsci.2018.07.087.

14 P. F. Andrade, A. F. de Faria, S. R. Oliveira, M. A. Z. Arruda and M. d. C. Gonçalves, Improved antibacterial activity of nanofiltration polysulfone membranes modified with silver nanoparticles, *Water Res.*, 2005, **81**, 333–342, DOI: 10.1016/j.watres.2015.05.006.

15 H. S. Lee, S. J. Im, J. H. Kim, H. J. Kim, J. P. Kim and B. R. Min, Polyamide thin-film nanofiltration membranes containing TiO_2 nanoparticles, *Desalination*, 2008, **219**, 48–56, DOI: 10.1016/j.desal.2007.06.003.

16 L. Valentino, M. Matsumoto, W. R. Dichtel and B. J. Mariñas, Development and Performance Characterization of a Polyimine Covalent Organic Framework Thin-Film Composite Nanofiltration Membrane, *Environ. Sci. Technol.*, 2017, **51**, 14352–14359, DOI: 10.1021/acs.est.7b04056.

17 Z. Yang, Z. W. Zhou, H. Guo, Z. Yao, X. H. Ma, X. Song, S. P. Feng and C. Y. Tang, Tannic Acid/Fe(3+) Nanoscaffold for Interfacial Polymerization: Toward Enhanced Nanofiltration Performance, *Environ. Sci. Technol.*, 2018, **52**, 9341–9349, DOI: 10.1021/acs.est.8b02425.

18 X. Li, A. Sotto, J. Li and B. Van der Bruggen, Progress and perspectives for synthesis of sustainable antifouling composite membranes containing in situ generated nanoparticles, *J. Membr. Sci.*, 2017, **524**, 502–528, DOI: 10.1016/j.memsci.2016.11.040.

19 J. K. Holt, H. G. Park, Y. Wang, M. Stadermann, A. B. Artyukhin, C. P. Grigoropoulos, A. Noy and O. Bakajin, Fast mass transport through sub-2-nanometer carbon nanotubes, *Science*, 2006, **312**, 1034–1037, DOI: 10.1126/science.1126298.

20 L. F. Dumée, K. Sears, J. Schütz, N. Finn, C. Huynh, S. Hawkins, M. Duke and S. Gray, Characterization and evaluation of carbon nanotube bucky-paper membranes for direct contact membrane distillation, *J. Membr. Sci.*, 2010, **351**, 36–43, DOI: 10.1016/j.memsci.2010.01.025.

21 P. S. Goh, A. F. Ismail and B. C. Ng, Directional alignment of carbon nanotubes in polymer matrices: contemporary approaches and future advances, *Compos. Appl. Sci. Manuf.*, 2014, **56**, 103–126, DOI: 10.1016/j.compositesa.2013.10.001.

22 H. J. Kim, Y. Baek, K. Choi, D.-G. Kim, H. Kang, Y.-S. Choi, J. Yoon and J.-C. Lee, The improvement of antibiofouling properties of a reverse osmosis membrane by oxidized CNTs, *RSC Adv.*, 2014, **4**, 32802–32810, DOI: 10.1039/c4ra06489e.

23 P. C. P. Watts, P. K. Fearon, W. K. Hsu, N. C. Billingham, H. W. Kroto and D. R. M. Walton, Carbon nanotubes as polymer antioxidants, *J. Mater. Chem.*, 2003, **13**, 491–495, DOI: 10.1039/b211328g.

24 J.-H. Choi, J. Jegal and W.-N. Kim, Fabrication and characterization of multi-walled carbon nanotubes/polymer blend membranes, *J. Membr. Sci.*, 2006, **284**, 406–415, DOI: 10.1016/j.memsci.2006.08.013.

25 M. J. Maryam Amini, Ahmad Rahimpour, Synthesis of novel thin film nanocomposite (TFN) forward osmosis membranes using functionalized multi-walled carbon nanotubes, *J. Membr. Sci.*, 2013, **435**, 233–241, DOI: 10.1016/j.memsci.2013.01.041.

26 M. H.-O. Rashid and S. F. Ralph, Carbon Nanotube Membranes: Synthesis, Properties,and Future Filtration Applications, *Nanomaterials*, 2017, **7**, 99, DOI: 10.3390/nano7050099.

27 S. M. Xue, Z. L. Xu, Y. J. Tang and C. H. Ji, Polypiperazine-amide Nanofiltration Membrane Modified by Different Functionalized Multiwalled Carbon Nanotubes (MWCNTs), *ACS Appl. Mater. Interfaces*, 2016, **8**, 19135–19144, DOI: 10.1021/acsami.6b05545.

28 V. Vatanpour, S. S. Madaeni, R. Moradian, S. Zinadini and B. Astinchap, Fabrication and characterization of novel antifouling nanofiltration membrane prepared from oxidized multiwalled carbon nanotube/polyethersulfone nanocomposite, *J. Membr. Sci.*, 2011, **375**, 284–294, DOI: 10.1016/j.memsci.2011.03.055.

29 H. Zarrabi, M. E. Yekavalangi, V. Vatanpour, A. Shockravi and M. Safarpour, Improvement in desalination performance of thin film nanocomposite nanofiltration membrane using amine-functionalized multiwalled carbon nanotube, *Desalination*, 2016, **394**, 83–90, DOI: 10.1016/j.desal.2016.05.002.

30 X.-H. Ma, H. Guo, Z. Yang, Z.-K. Yao, W.-H. Qing, Y.-L. Chen, Z.-L. Xu and C. Y. Tang, Carbon nanotubes enhance permeability of ultrathin polyamide rejection layers, *J.*

Membr. Sci., 2019, **570–571**, 139–145, DOI: 10.1016/j.memsci.2018.10.055.

31 H. Wu, H. Sun, W. Hong, L. Mao and Y. Liu, Improvement of Polyamide Thin Film Nanocomposite Membrane Assisted by Tannic Acid-Fe(III) Functionalized Multiwall Carbon Nanotubes, *ACS Appl. Mater. Interfaces*, 2017, **9**, 32255–32263, DOI: 10.1021/acsami.7b09680.

32 G. N. B. Baroña, M. Choi and B. Jung, High permeate flux of PVA/PSf thin film composite nanofiltration membrane with aluminosilicate single-walled nanotubes, *J. Colloid Interface Sci.*, 2012, **386**, 189–197, DOI: 10.1016/j.jcis.2012.07.049.

33 J. n. Shen, C. c. Yu, H. m. Ruan, C. j. Gao and B. Van der Bruggen, Preparation and characterization of thin-film nanocomposite membranes embedded with poly(methyl methacrylate) hydrophobic modified multiwalled carbon nanotubes by interfacial polymerization, *J. Membr. Sci.*, 2013, **442**, 18–26, DOI: 10.1016/j.memsci.2013.04.018.

34 J. Zheng, M. Li, K. Yu, J. Hu, X. Zhang and L. Wang, Sulfonated multiwall carbon nanotubes assisted thin-film nanocomposite membrane with enhanced water flux and anti-fouling property, *J. Membr. Sci.*, 2017, **524**, 344–353, DOI: 10.1016/j.memsci.2016.11.032.

35 V. Vatanpour, M. Esmaeili and M. H. D. A. Farahani, Fouling reduction and retention increment of polyethersulfone nanofiltration membranes embedded by amine-functionalized multi-walled carbon nanotubes, *J. Membr. Sci.*, 2014, **466**, 70–81, DOI: 10.1016/j.memsci.2014.04.031.

36 W. Yang, H. Xu, W. Chen, Z. Shen, M. Ding, T. Lin, H. Tao, Q. Kong, G. Yang and Z. Xie, A polyamide membrane with tubular crumples incorporating carboxylated single-walled carbon nanotubes for high water flux, *Desalination*, 2020, **479**, DOI: 10.1016/j.desal.2020.114330.

37 Z. J. Santanu Karan and A. G. Livingston, Sub–10 nm polyamide nanofilms with ultrafast solvent transport for molecular separation, *Science*, 2014, **348**, 1347–1351.

38 S. S. Madaeni, K. Derakhshandeh, S. Ahmadi, V. Vatanpour and S. Zinadini, Effect of modified multi-walled carbon nanotubes on release characteristics of indomethacin from symmetric membrane coated tablets, *J. Membr. Sci.*, 2012, **389**, 110–116, DOI: 10.1016/j.memsci.2011.10.021.

39 J. Kathi, K.-Y. Rhee and J. H. Lee, Effect of chemical functionalization of multi-walled carbon nanotubes with 3-aminopropyltriethoxysilane on mechanical and morphological properties of epoxy nanocomposites, *Compos. Appl. Sci. Manuf.*, 2009, **40**, 800–809, DOI: 10.1016/j.compositesa.2009.04.001.

40 C. Y. Tang, Y.-N. Kwon and J. O. Leckie, Effect of membrane chemistry and coating layer on physiochemical properties of thin film composite polyamide RO and NF membranes, *Desalination*, 2009, **242**, 149–167, DOI: 10.1016/j.desal.2008.04.

41 Q.-F. An, W.-D. Sun, Q. Zhao, Y.-L. Ji and C.-J. Gao, Study on a novel nanofiltration membrane prepared by interfacial polymerization with zwitterionic amine monomers, *J. Membr. Sci.*, 2013, **431**, 171–179, DOI: 10.1016/j.memsci.2012.12.043.

42 X.-H. Ma, Z.-K. Yao, Z. Yang, H. Guo, Z.-L. Xu, C. Y. Tang and M. Elimelech, Nanofoaming of Polyamide Desalination Membranes To Tune Permeability and Selectivity, *Environ. Sci. Technol. Lett.*, 2018, **5**, 123–130, DOI: 10.1021/acs.estlett.8b00016.

43 H. Zhao, S. Qiu, L. Wu, L. Zhang, H. Chen and C. Gao, Improving the performance of polyamide reverse osmosis membrane by incorporation of modified multi-walled carbon nanotubes, *J. Membr. Sci.*, 2014, **450**, 249–256, DOI: 10.1016/j.memsci.2013.09.014.

44 Z. Tan, S. Chen, X. Peng, L. Zhang and C. Gao, Polyamide membranes with nanoscale turing structures for water purification, *Science*, 2018, **360**, 518–521.

45 T. Saito, K. Matsushige and K. Tanaka, Chemical treatment and modification of multi-walled carbon nanotubes, *Phys. B Condens. Matter*, 2002, **323**, 280–283, DOI: 10.1016/s0921-4526(02)00999-7.

46 S. Veríssimo, K. V. Peinemann and J. Bordado, Influence of the diamine structure on the nanofiltration performance, surface morphology and surface charge of the composite polyamide membranes, *J. Membr. Sci.*, 2006, **279**, 266–275, DOI: 10.1016/j.memsci.2005.12.014.

47 B. Van der Bruggen, J. Schaep, D. Wilms and C. Vandecasteele, Influence of molecular size, polarity and charge on the retention of organic molecules by nanofiltration, *J. Membr. Sci.*, 1999, **156**, 29–41, DOI: 10.1016/S0376-7388(98)00326-3.

48 Z. Mao and S. B. Sinnott, A Computational Study of Molecular Diffusion and Dynamic Flow through Carbon Nanotubes, *J. Phys. Chem. B*, 2000, **104**, 4618–4624.

49 I. J. Roh, A. R. Greenberg and V. P. Khare, Synthesis and characterization of interfacially polymerized polyamide thin films, *Desalination*, 2006, **191**, 279–290, DOI: 10.1016/j.desal.2006.03.004.

50 S.-T. Nam and M.-J. Han, Thermodynamic and rheological variation in polysulfone solution by PVP and its effect in the preparation of phase inversion membrane, *J. Membr. Sci.*, 2002, **202**, 55–61.

51 Y. Kang, M. Obaid, J. Jang and I. S. Kim, Sulfonated graphene oxide incorporated thin film nanocomposite nanofiltration membrane to enhance permeation and antifouling properties, *Desalination*, 2019, **470**, DOI: 10.1016/j.desal.2019.114125.

52 M. Safarpour, V. Vatanpour, A. Khataee and M. Esmaeili, Development of a novel high flux and fouling-resistant thin film composite nanofiltration membrane by embedding reduced graphene oxide/TiO$_2$, *Sep. Purif. Technol.*, 2015, **154**, 96–107, DOI: 10.1016/j.seppur.2015.09.039.

53 L. Zhang, M. Zhang, J. Lu, A. Tang and L. Zhu, Highly permeable thin-film nanocomposite membranes embedded with PDA/PEG nanocapsules as water transport channels, *J. Membr. Sci.*, 2019, **586**, 115–121, DOI: 10.1016/j.memsci.2019.05.065.

54 J.-J. Wang, H.-C. Yang, M.-B. Wu, X. Zhang and Z.-K. Xu, Nanofiltration membranes with cellulose nanocrystals as an interlayer for unprecedented performance, *J. Mater. Chem. A*, 2017, **5**, 16289–16295, DOI: 10.1039/c7ta00501f.